A New Restructured Shaded Pole Induction Motor– 3D Finite Element Analysis and Experimental Verification

Sadegh Shamlou[1] , Mojtaba Mirsalim[2]

[1]Department of Electrical Engineering, K.N.Toosi University of Technology,Tehran, Iran.Email:shamlou@eetd.kntu.ac.ir
[2]Department of Electrical Engineering, Amirkabir University of Technology, Tehran, Iran. Email:mirsalim@aut.ac.

Abstract

Shaded pole induction motors, despite the simplicity and low cost, are difficult to analyze particularly in the equivalent circuit methods, due to the asymmetric structure, saturation, harmonics, inaccurate estimation of leakage inductances and skew. Hence, 3D numerical methods could be very useful in the design and optimization stage. This paper presents the 3D transient finite element analysis (3DTFEM) of a 1/60HP, 2-pole prototyped, restructured shaded pole induction motor that has been designed and optimized using genetic algorithm technique. Experimental test has been carried out by a hysteresis brake dynamometer to determine the motor performance. Detailed comparisons among 2D, and 3D finite-element analysis, and experimental results are presented, which confirm the potentials of the new restructured shaded pole motor to achieve lower cost and higher efficiency objectives than the previous designs.

Keywords: 3D Finite Element Analysis, Restructured Shaded Pole Induction Motor, Skew, GA Optimization.

© 2015 IAUCTB-IJSEE Science. All rights reserved

1. Introduction

Shaded pole induction motors (SPIM) are generally being used in a wide variety of small power applications such as small fans, and small water pumps. In spite of maintenance free characteristics, the low efficiency of this motor has posed special challenges to designers and discouraged the selection of the SPIM in some new applications. This problem has been addressed in a recent work that has developed an optimum SPIM [1].

Previous investigation by authors has shown that minimum of raw material and operating cost can be achieved using SPIMs by introducing a new stator structure to increase efficiency and reduce raw material usage. A cost-optimized SPIM was designed for a small water pump application using a genetic algorithm that provides an effective means for global optimization of SPIM designs using transient two-dimensional finite element analysis (2-D FEA) [1].

In the 2-D FEA, three parameters of rotor skewing, end ring resistance and inductance, and the leakage inductances of winding overhangs were not considered directly. The methods of calculation of these parameters have been addressed in some works [2]-[4]. The 2-D multi-slice FEA has been used to consider the skew effect [5]. However, these parameters can be considered in the 3-D FEA, which has more accuracy to calculate performance characteristics.Until now, only few works used 3-D FEA to analyze SPIMs. Sadeghi, and others [6] implemented 3-D FEA to show the complexity and importance of the space harmonics in "C" frame shaded pole motors. However, 3-D FEA is a time-consuming tool, which is not proper for optimization process but its results are most reliable due to comprehensive modeling capability. In the current research, the authors have extensively used the 3-D FEA in the analysis process.

This paper presents the 3-D FEA of a 1/60-HP 2-pole shaded pole motor that has been optimized using genetic algorithm in [1]. The 3-D FEA and experimental testing of the motor has been carried out to evaluate its performance capabilities including higher efficiency, improved torque-speed characteristic, and lower cost. The main goal is to

present the key results from experimental tests as a means of exploring the strengths and weaknesses of the new optimum restructured SPIM.

1. The New Restructured Shaded pole Induction Motor

Fig. 1 shows the optimum restructured SPIM that has been designed to achieve minimum raw material and operating cost [1]. The motor was originally designed to deliver 1/60 HP at the nominal speed of 2450 r/min. As it can been seen from the figure, the stator has two parts that are assembled after inserting the two coils. The key parameters and dimensions for the stator and rotor are tabulated in Table (1).

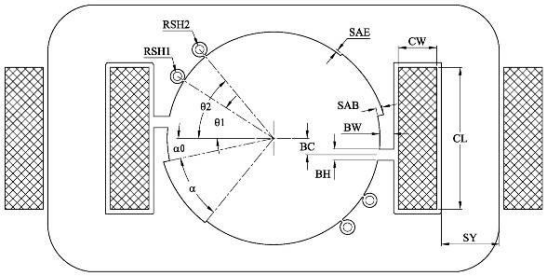

Fig. 1. The optimum restructured SPIM proposed and designed in [1]

Table.1.
Stator and rotor dimensions for the optimum restructured SPIM

Parameter	*Description*	*Values*	*Units*
SY	Stator yoke	12	mm
Lfe	Stator and rotor stack length	16	mm
CL	Coil length	30.5	mm
CW	Coil width	8.1	mm
N	Turns of stator coil	1650	
WG	Wire gauge	0.22	mm
BW	Bridge air-gap width	3.08	mm
BH	Bridge air-gap height	0.36	mm
BC	Bridge air-gap center position	-2.7	mm
α	Angle of stepped air-gap	48.3	rad
α0	Starting Angle - Stepped Air-gap	3.06	rad
SAB	Initial air-gap step	0.82	mm
SAE	Final air-gap step	0.75	mm
θ1	Angle of shading 1	35.3	rad
θ2	Angle of shading 2	50.8	rad
RSH1	Radius of shadings 1	1.2	mm
RSH2	Radius of shadings 2	1.45	mm
RD	Rotor diameter	22.15	mm
NR	Number of rotor slots	26	
RSH	Rotor slot height	5.1	mm
RTW	Rotor tooth width	2.05	mm

2. The 2-D Optimization Results

Fig. 2 shows the flux lines and flux density in the optimum restructured SPIM. The details of the cost parameters for the optimum design and the conventional model are compared in Table (2) [1]. Here, we clearly observe the significant reduction in total cost of the optimum design, and hence the validity of the optimized restructured model is confirmed.The starting torque, the output power, the input current, efficiency, and power factor are usually the main performance criteria for SPIMs. These criteria for the optimum design of the restructured SPIM are summarized in Table (3).By using shorter path for the main flux in the optimum design of the restructured SPIM, we have a significant decrease in the usage of steel (by 6%) and copper (by 3%) and therefore, the raw material cost will decrease accordingly. In addition, the larger rotor diameter delivers more output torque. Furthermore, the winding resistance has reduced by 25% compared to the conventional model, and this is the main reason that the efficiency increases by more than seven percent [1].

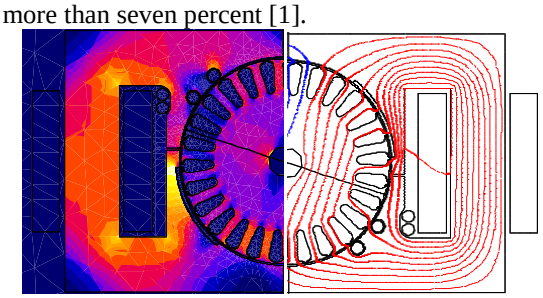

Fig. 2. Flux density and magnetic field distribution of the optimum restructured SPIM design

Table.1.
cost parameters of the optimum restructured SPIM and their respective changes compared to the conventional model [1]

Cost Parameters	*Optimum Design*	*Reduction*
Raw material Cost	1.857 $	7.2%
Operating cost	39.68 $	29%

Table.2.
Measured performances of the optimum SPIM

Parameters	*Optimum design*
Output power	12.40 W
Efficiency	25%
Input current	0.376 A
Input power	49.60 W
Input VAR	66.13 VAR
Power factor	0.60
Starting torque	0.024 N.m

3. The 3-D FEA

In the 2-D FEA calculations, three parameters of rotor skewing, end ring resistance and inductance, and the leakage inductances of winding overhangs were not considered directly. However, these parameters are considered in the 3-D FEA, which is more accurate in calculation of performance characteristics. The field equations in terms of current density J, vector potential A, and scalar potential V can be written as in the following [8]:

$$J = \sigma E = -\sigma \frac{\partial A}{\partial t} - \sigma \nabla \phi \quad (1)$$

$$\nabla \times \left(\frac{1}{\mu} \nabla \times A \right) = J. \quad (2)$$

$$\nabla \times \left(\frac{1}{\mu} \nabla \times A \right) + \sigma \frac{\partial A}{\partial t} + \sigma \nabla \phi = 0. \quad (3)$$

where ϕ is the reduced electric scalar potential, μ permeability, σ electric conductivity [S/m].

In this paper, a transient 3-D FEA is applied on optimum restructured SPIM as shown in Fig. 3. Dynamic characteristics of the optimum restructured SPIM calculated by 3-D FEA and 2-D FEA are shown in Fig. 4. As it can be seen, the 2-D results have acceptable approximations in calculating performances.Fig. 5 shows the radial flux density in the middle of the air-gap at rated speed using both 2-D and 3-D FE analysis. The excellent agreement between these two waveforms builds confidence in the accuracy of the optimization process. The flux density waveform in the middle of the air gap contains notable harmonic components. As a result, the ripple in the torque is significant.

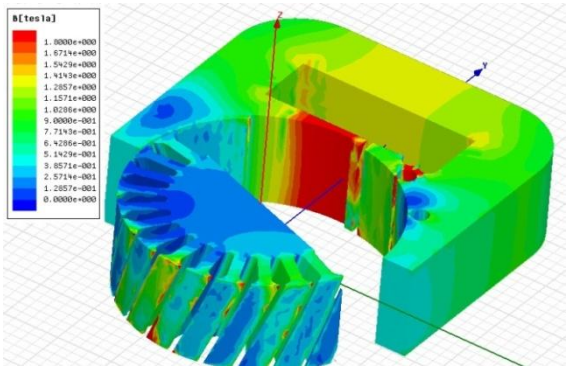

(a)

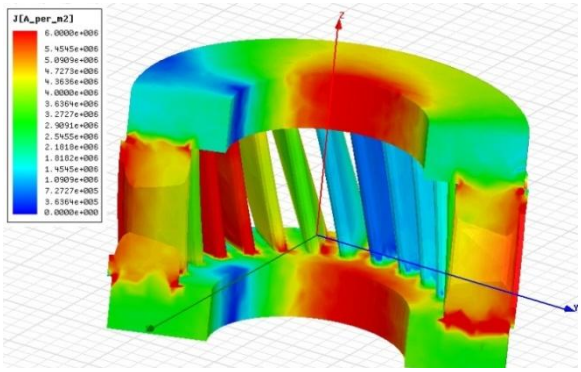

(b)

Fig. 3. (a) Flux density distribution and (b) Rotor cage current density of the optimum restructured SPIM

4. Experimental Results

This section provides a summary of the key experimental results, including parameter measurements and comparisons between the experimental results and both 2-D FEA and 3-D FEA results.

Fig. 6 shows the laminated stator core, while the stator assembly along with its concentrated winding coils during fabrication is shown in Fig. 7. Two dovetail joints hold the two parts of stator together. Fig. 8 shows a different view of the optimum SPIM, where the stator and rotor has been assembled in the aluminum bottom part of the frame.

Fig. 9 shows a part of the test set-up. The optimum restructured SPIM is coupled to a dynamometer that uses a hysteresis load. An in-line torque transducer measures the torque and speed.

The measured value of the resistance of stator winding at the room temperature is approximately 112 Ω. The measured phase inductance is approximately 1.65 H, which is higher than the 1.35 H predicted by the 2-D FEA. The discrepancy is mostly due to the end-winding leakage inductance that is not included in the 2-D FEA. On the other hand, the 3-D FEA prediction of 1.70 H approximately coincides with the measured value.

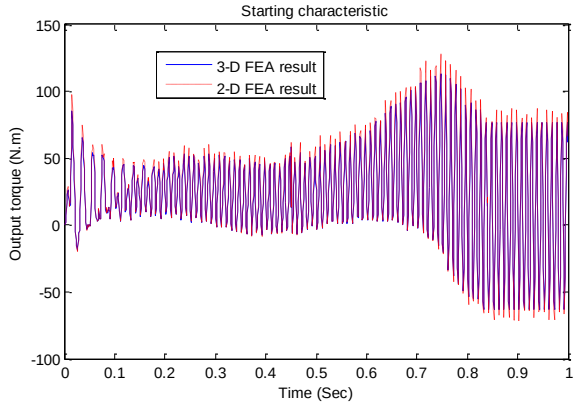

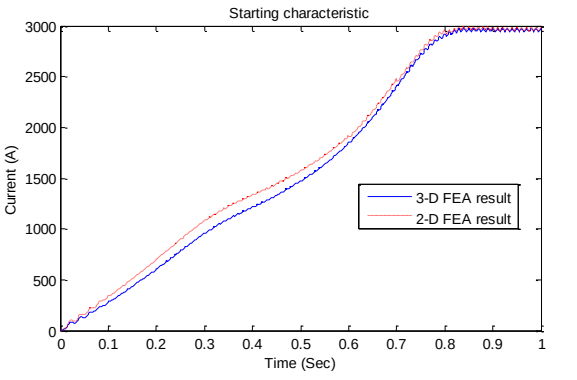

(b)

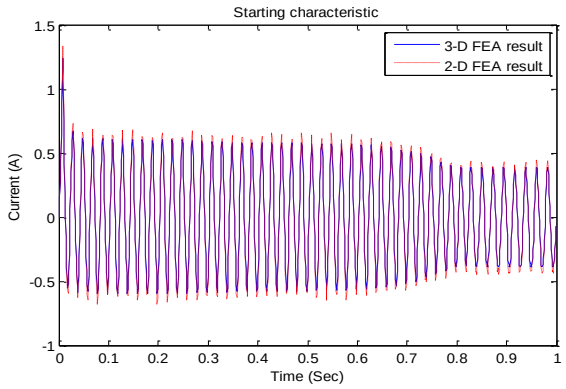

(c)

Fig. 4. Dynamic characteristics of the optimum restructured SPIM at the no-load starting, (a) Torque, (b) Speed, (c) Current

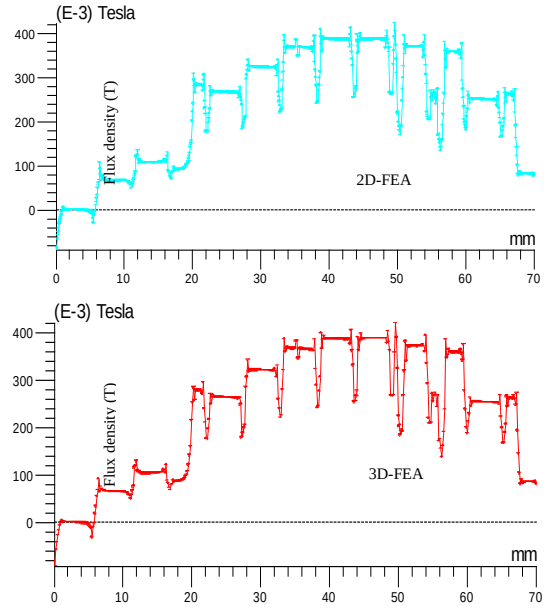

Fig. 5. 2-D FEA and 3-D FEA flux density in the middle of air-gap for the optimum restructured SPIM

Fig. 6. Optimum motor stator core

Fig. 7. Stator and its windings during the assembly process

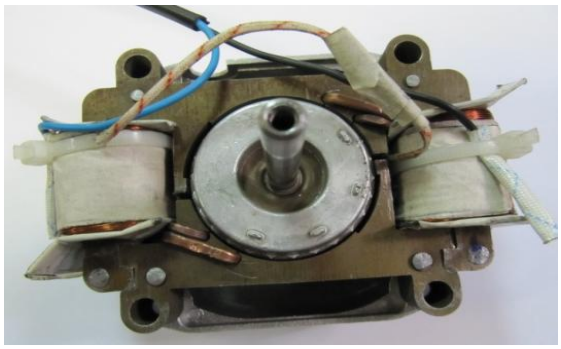

Fig. 8. Close-up view of the motor after stator-rotor assembly in the aluminum bottom part of the frame

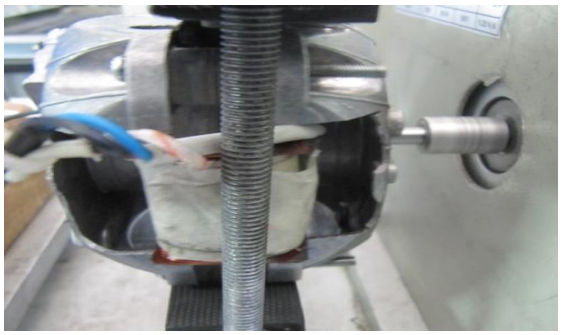

Fig. 9. Dynamometer test of the optimum restructured SPIM

Table (4). compares the optimum restructured SPIM experimental parameters at rated speed with the 3-D FEA results, which demonstrate excellent agreement. The measured input current is slightly higher than the FEA result due to the given properties of steel, the predicted winding temperature, and the effects of non-ideal assembly process. The harmonic spectra of the input current waveform predicted by the 3-D FEA and shown in Fig. 10 consist almost entirely of the fundamental and the third harmonic components.

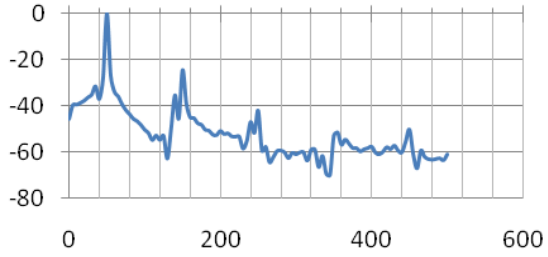

Fig. 10. 20dB FFT of input current

Table.3.
Comparison of Measured and 3-D FEA results of the optimum Restructured SPIM

Parameters	*Measured results*	*3-D FE results*
Output power	12.40 W	12.51 W
Efficiency	25%	25.3%
Input current	0.376 A	0.363 A
Input power	49.60 W	48.68 W
Input VAR	66.13 VAR	63.24 VAR
Power factor	0.60	0.61
Starting torque	0.024 N.m	0.025 N.m

Comparisons of the measured and 3-D FEA predictions of machine torque versus speed curves and the corresponding power versus speed curves are shown in Figs. 11 and 12, respectively. The figures show that there is a very good agreement between the measured and FEA results. These results are very significant since they confirm that the prototype machine has achieved a no-dip torque specification and has a higher power density capability.It is deduced from Fig. 11 that the measured torque is slightly smaller than the predicted 3-D FEA result at low speeds. This is consistent with the lower value of inductance in the prototype machine, as previously discussed.

Fig. 13 shows a comparison of the measured and calculated machine efficiency versus speed on the torque or power envelopes. The 3-D FEA prediction and measured results approximately agree very closely over the tested speed range.

The measured efficiency of the prototype machine is larger than 24% at rated speeds, confirming successful enhancement of the produced torque that is obliged by the larger rotor diameter. This is very significant since efficiency has been one of the key potential obstacles in using SPIMs for general applications.

As can be seen in Fig. 13, the calculated efficiency of the optimized restructured SPIM is slightly bigger than the measured value in a large portion of speed range. To investigate this difference, it should be noted that more than 75% of losses in this type of motors are due to stator winding and rotor resistances [8]. The temperatures of the stator winding and the rotor bars change during the dynamometer load test. Therefore, the SPIM efficiency is very sensitive to temperature due to its effect on the stator winding and rotor resistances and consequently on the copper losses. This is the main reason for the difference between the measured and predicted efficiencies.

Fig. 14 shows the measured and the predicted power factors versus speed for the prototype motor. The predicted and measured power factors agree very well and they show that the machine power factor is nearly 0.6 over most of the speed range.

5. Conclusion

A 1/60-HP 2-pole restructured SPIM has been successfully designed, fabricated, and tested to achieve a low cost and high efficiency performance. The 3-D finite element analysis was extensively used during the analysis process. Important motor performance issues including output torque and power were analyzed in detail. Experimental results obtained from the optimum restructured SPIM were used to evaluate the accuracy of the 3-D FEA, which was implemented for parameters calculations. Comparisons of motor parameters and performance obtained from the 3-D FEA with the experimental tests demonstrated very good agreement. Average discrepancy between 3-D FEA and experimental results is 2.18%. The test results have validated the potentials of the optimum restructured SPIM such as lower cost and higher efficiency compared to the conventional designs.

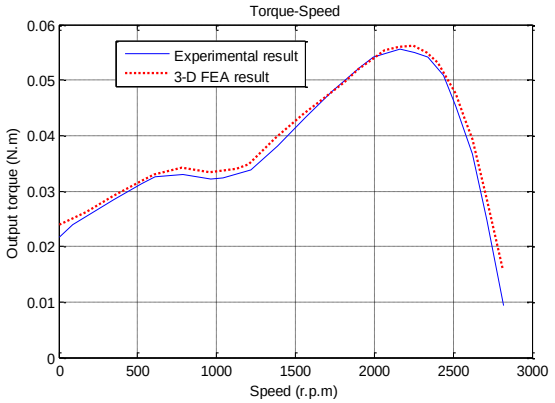

Fig. 11. Comparison of the measured and calculated output torque versus speed curves

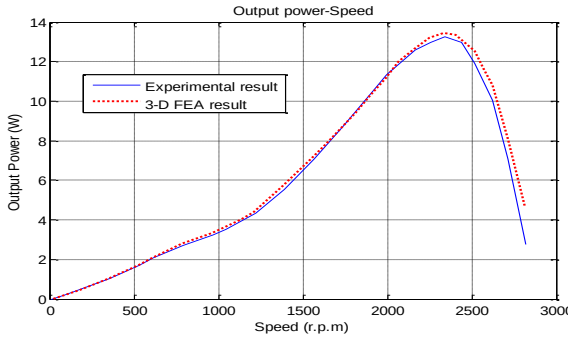

Fig. 12. Comparison of the measured and calculated output power versus speed curves

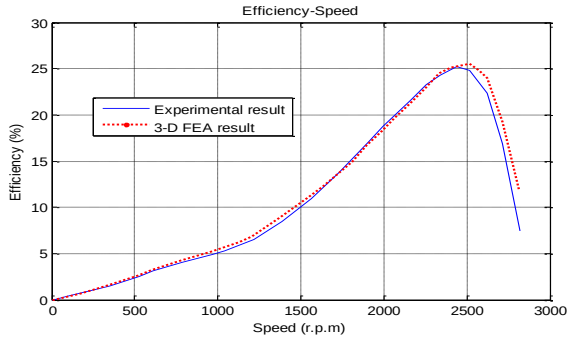

Fig. 13. Comparison of the measured and calculated efficiency versus speed

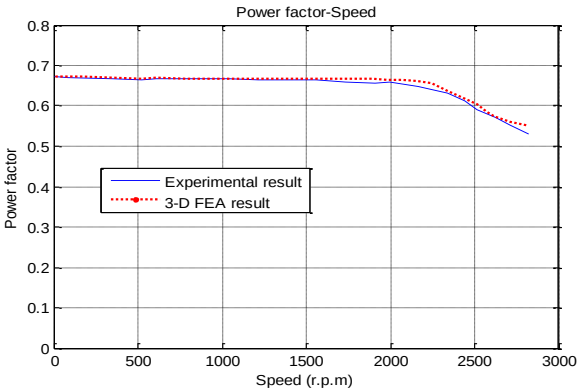

Fig. 14. Comparison of the measured and calculated power factor versus speed curves

References

[1] S. Shamlou, M. Mirsalim, Global Optimization of Restructured Shaded Pole Induction Motors Based on Genetic Algorithm Method, International Review of Electrical Engineering (I.R.E.E.), Vol. 6, N. 4, July-August, pp. 1675-1682, 2011.

[2] K.S. Lock, Analysis of the Steady-State Performance of the Reluctance-Augmented Shaded-Pole Motors, Transaction on Power Apparatus and Systems, vol. pas-103, no.9, September, pp.2625-2632, 1984.

[3] P. H. Trickey, An Analysis of the Shaded Pole Motor, AIEE Transaction, vol. 45, pp.1007-1014, 1936.

[4] De Weerdt, R. Belmans, Squirrel cage inductance motor end effects using 2D and 3D finite element, International Conference on Electrical Machine and Drives, pp62-66, 1995.

[5] D. Zhou, C. B. Rajanathan, A. T. Sapeluk, R. Egin, Transient simulation of the shaded pole motor based upon a multi-slice finite-element model, 9th International Conference on Electrical Machines And Drives, no. 468, pp. 30-34, 1999.

[6] H. Sadeghi, E.F Richards, Evaluation of space harmonics in a "C" type shaded pole motor and sensitivity study of its stalled torque with respect to its design parameters, Industry Applications Conference, vol. 1, pp. 759-766,1995.

[7] A. T. DE. Almeida, F. J. T. E. Ferreira, J. A. C. Fong, Standards for efficiency of electric motor,IEEE Industrial Application Magazine, Nov. 2010.

[8] J. Pyrhonen, T. Jokinen, V. Hrabovcova, Design of Rotating Electrical Machines, John Wiley & Sons, Ltd. ISBN: 978-0-470-69516-6, pp9-10, 2008.